ENHANCEMENT IN GAS PUMPING IN A SQUARE CHANNEL WITH TWO-STAGE CORONA WIND GENERATOR

A. K. M. Monayem H. Mazumder* and F. C. Lai†

University of Oklahoma
865 Asp Ave.
Norman, OK 73019, USA
flai@ou.edu

Abstract -- **In this study flow field inside a square channel with a two-stage electrohydrodynamic (EHD) gas pump has been critically examined by experimental measurement and numerical simulation. The EHD gas pump with 28 emitting electrodes in each stage is tested for a wide range of operating voltages starting from the corona onset voltage up to 28 kV for further improvement in its performance over a single-stage one. It has been shown that the two-stage EHD gas pump can produce and sustain gas flows with a maximum velocity of 5 m/s. Its maximum performance of 34 L/s/W is better than that of conventional cooling fans used in personal computers. The implication for its application in thermal management and heat transfer enhancement has also been discussed.**

Index Terms—**Electrostatics, Fans, Fluid Dynamics, Modeling, Numerical Simulation, Pumps, Space Charge, Velocity Measurement.**

NOMENCLATURE

A	surface area of the grounded plate, [m^2]
b	ion mobility, [m^2/V·s]
D	channel width, [m]
I	total corona current, [A]
p	pressure, [Pa]
p_i	pressure at the inlet, [Pa]
Re	Reynolds number, u_iD/v
u	x-component of velocity, [m/s]
u_e	characteristic velocity of corona wind, $\sqrt{\rho_{c0}V_0/\rho}$
u_i	inlet air velocity, [m/s]
v	y-component of velocity, [m/s]
V	electric potential, [V]
V_0	electric potential at the wire, [V]
w	z-component of velocity, [m/s]
$\bar{x}$	dimensionless length in x-direction, x/D
ε	electric permitivity, [F/m]
v	kinematic viscosity, [m^2/s]
ρ	density of air, [kg/m^3]
ρ_c	space charge density, [C/m^3]
$\bar{\rho}_c$	dimensionless space charge density, ρ_c / ρ_{c0}
ρ_{c0}	space charge density at the wire tip [C/m^3]

INTRODUCTION

The use of electrical field to enhance heat and mass transfer has been a subject of great interest for many decades. This enhancement mechanism is based on the use of electrical body force to induce a secondary flow or simply create a flow where none would otherwise exist. To produce such flow, it involves two electrodes; one has a large curvature (such as a needle or a small diameter wire) and one with a small curvature (such as a plate). The one with a large curvature ensures forming a high electric potential gradient around the electrode, which leads to the generation of corona discharge in the narrow region between the two electrodes. Gas molecules are ionized by the intense electrical field. Driven by Coulomb force, these ions migrate to the grounded electrode. During the migration, these ions transfer their momentum to neutral molecules via collision. This creates a bulk flow, which is usually called ionic wind or corona wind [1]. Thus, corona wind is produced by an electrode charged with a direct current (either positive or negative) at a sufficiently high voltage (usually in the kV range). While the applied voltage may be high, the current involved is usually very small (in the μA to mA range), which makes the power required considerably small. This has become one of the most attractive features for the electrohydrodynamic (EHD) technique described above. In recent years, there has been a surge of interest in the application of EHD technique for pumping dielectric liquids [2]. Because of the low power consumption and no moving part involved, EHD pumps have been considered a valuable alternative for conventional pumps.

EHD techniques have been applied to a wide range of engineering fields. For example, electrostatic precipitators have been used to control particle emission in manufacturing and power industries [3]. In addition, in food industry, corona wind has become a novel method to enhance the drying process [4-6]. EHD actuators are used in the aerospace industry to reduce the drag of an aircraft or to stabilize the air flow [7-11]. In thermal management of electronic systems, corona wind can produce a substantial increase in the heat transfer coefficient [12-14]. Recently, as microelectronics has become an emerging technology, EHD techniques have also played an important role in the development of microelectromechanical system (MEMS) [15].

Electrohydrodynamic technique has many advantages. First, this technique converts electric energy directly into kinetic energy without any moving part, and therefore the maintenance cost can be greatly reduced. Secondly, this

technique is operated electrically and it can be incorporated into the existing systems to be conveniently controlled by a computer. Thirdly, it is highly compatible with chips and chip-level structures. Thus, miniaturization can be easily realized [16]. Lastly and most importantly, its power consumption is usually very small, which makes this technique particularly attractive from the energy point of view. Its only disadvantage is the generation of ozone that might be harmful to human beings. However, ozone generation can be effectively controlled and minimized if the emitting electrodes are kept clean all the time [17].

Although EHD gas pumps have been shown promising [18-24], it has been observed that their application may be confined to a short distance [25]. It has been speculated that using a two-stage EHD gas pump may help to extend the range of their application. In this approach, the first stage of the pump is used to initiate the flow and the second stage to boost the flow. Thus the objective of the present study is to address this important issue in the EHD gas pump design. To aid the investigation, experimental measurements and numerical simulations have been conducted.

EXPERIMENTAL SETUP

The schematic of the experimental setup used is shown in Fig. 1. The main components are: EHD pump test unit, high voltage power supply, air velocity transducer, and data acquisition system (DAQ). The test channel was constructed from Plexiglas of 0.635 cm (¼ in.) thick. The inner dimensions of the channel were 10.2 cm by 10.2 cm by 76.2 cm (4 in. by 4 in. by 30 in.). The dimensions of the wire-electrode and system configuration are shown in Fig. 2. A copper wire of 20 GA was first bent and welded to form the electrode loop, which was then flush mounted on the inner wall of the channel. Additional 2.54-cm-long (1-inch-long) copper wires of the same size were welded to the base loop to serve as emitting electrodes. They were evenly distributed over the channel walls and altogether there were 28 emitting electrodes in each stage (7 on each side of the wall). For the bottom stage, a 1.27–cm (0.5-inch) wide and 0.635 mm (0.025 in.) thick copper strip was flush mounted on all four sides of the inner wall to serve as the grounded electrode. For the top stage, three sizes of the grounded electrode were available. They are 1.27, 2.54, and 5.08 cm wide (0.5, 1, and 2 in. wide), respectively. For each stage, the gap between the tips of the emitting electrodes and the grounded plate was fixed at 3.81 cm (1.5 in.). The spacing between the electrode wire loops of the two stages was maintained at 15.24 cm (6 in.). The electrode assembly and the grounded plate were press-fitted to pre-cut grooves on the inner wall of the channel so that their surfaces were flushed with the channel wall. In this arrangement, the corona wind produced by the electrode will resemble that of a wall jet. It should be noted that the emitting electrodes were intended to align with the direction of primary flow to maximize its effect.

The wire electrode assembly was connected to a high voltage power supply (Bertan Associates, Series 205B-30R), which has a maximum capacity of 30 kV, and can be charged with a direct current of either positive or negative polarity. The plate was grounded at the same level as the power supply. Two ¼ inch NPT compression fittings were installed on the lower part (outlet section) of the channel to hold the velocity transducer (Omega FMA 902-I) in place to facilitate air flow measurements. The transducer, which can accurately measure air velocity from 0 to 500 ft/min (2.54 m/s) with an accuracy of 2.7% of full scale at room temperature. The velocity probe extended horizontally from channel wall allowing measurements be taken on three levels; 2.54 cm, 6.35 cm and 10.16 cm (1, 2.5 and 4 inches) downstream of the grounded plate of the bottom stage. A total of twenty one sampling points are evenly distributed at each level. The data acquisition system used is from National Instruments. The data sampling and collection are aided by the LabView program. The current signal received from the power supply and the velocity transducer are first calibrated and scaled to the correct values. A sampling rate of 1 Hz is used for all experiments. It is determined by systematic trials that 1 Hz is sufficient to capture the variations of electric and flow fields.
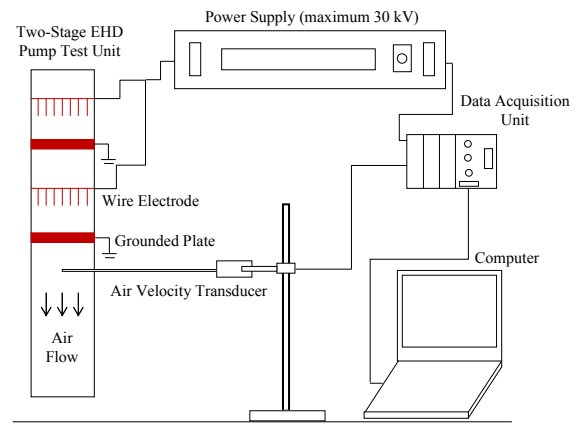

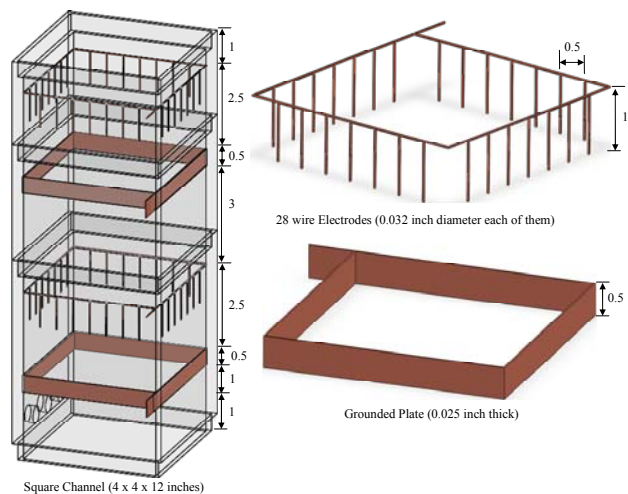Fig. 1 Schematic of the experimental setup.
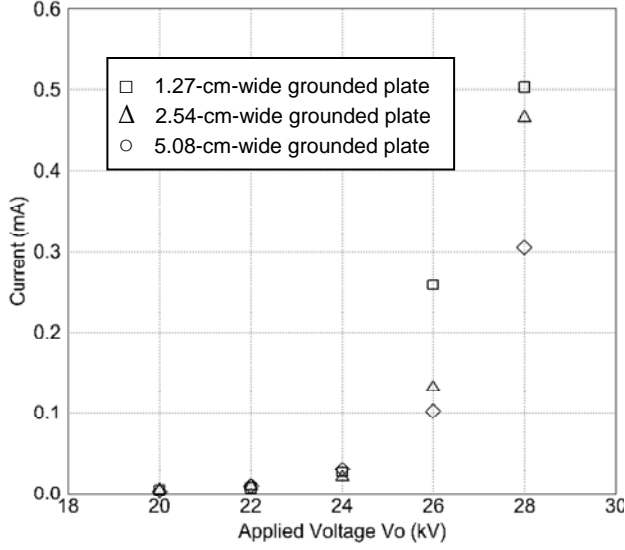

Fig. 2 Configuration of EHD pump test unit.

Fig. 3 V-I curves for the EHD gas pump tested.

Experiments are conducted with only positive corona discharge in this study. Negative corona discharge will be considered in the future study for comparison. To start the experiment, the applied voltage was gradually increased until a flow of air was detected by the velocity transducer. For the present setup, corona wind was too weak to be detected until the applied voltage was increased to 20 kV. The applied voltage was then increased incrementally by two kilovolts until sparkover occurred, which could be easily observed through a visible bright light and cracking sound that it produced. When it occurred (around 30 kV for the present study), electric field became unstable and fluctuated violently. As such, it was avoided to operate at this voltage. Typical V-I curves for the present experimental setup are shown in Fig. 3. As seen, the current produced by corona discharges increases with the applied voltage after the onset of corona. Also observed is that a two-stage EHD pump draws more current than that of one stage. It is interesting to note that at a higher applied voltage, a grounded plate with a smaller width in the top stage of the pump delivers more current than that with a larger width.

NUMERICAL FORMULATION AND PROCEDURE

For the problem considered, the governing equations of the electric field are given by Zhang and Lai [25]

$$\frac{\partial^2 V}{\partial x^2} + \frac{\partial^2 V}{\partial y^2} + \frac{\partial^2 V}{\partial z^2} = -\frac{\rho_c}{\varepsilon}, \tag{1}$$

$$\frac{\partial \rho_c}{\partial x}\frac{\partial V}{\partial x} + \frac{\partial \rho_c}{\partial y}\frac{\partial V}{\partial y} + \frac{\partial \rho_c}{\partial z}\frac{\partial V}{\partial z} = \frac{\rho_c^2}{\varepsilon}, \tag{2}$$

which can be readily derived from Maxwell equation, current continuity equation and Ohm's Law.

The corresponding boundary conditions are:

At the wire electrode	$V = V_0,$	(3a)
At the grounded plate	$V = 0,$	(3b)
At the inlet and outlet	$\frac{\partial V}{\partial z} = 0.$	(3c)

On the channel walls except the grounded plate,

$x = 0,$	$\frac{\partial V}{\partial x} = 0.$	(3d)
$y = 0,$	$\frac{\partial V}{\partial y} = 0.$	(3e)

On the symmetric surfaces,

$x = \frac{D}{2},$	$\frac{\partial V}{\partial x} = 0.$	(3f)
$y = \frac{D}{2},$	$\frac{\partial V}{\partial y} = 0.$	(3g)

The governing equations for the flow field are the continuity equation (Eq. (4)) and Navier-Stokes equations (Eqs. (5-7)), which are given below.

$$\frac{\partial u}{\partial x} + \frac{\partial v}{\partial y} + \frac{\partial w}{\partial z} = 0, \tag{4}$$

$$u\frac{\partial u}{\partial x} + v\frac{\partial u}{\partial y} + w\frac{\partial u}{\partial z} = -\frac{1}{\rho}\frac{\partial p}{\partial x} + \nu\left(\frac{\partial^2 u}{\partial x^2} + \frac{\partial^2 u}{\partial y^2} + \frac{\partial^2 u}{\partial z^2}\right) + \frac{\rho_c}{\rho}\frac{\partial V}{\partial x}, \tag{5}$$

$$u\frac{\partial v}{\partial x} + v\frac{\partial v}{\partial y} + w\frac{\partial v}{\partial z} = -\frac{1}{\rho}\frac{\partial p}{\partial y} + \nu\left(\frac{\partial^2 v}{\partial x^2} + \frac{\partial^2 v}{\partial y^2} + \frac{\partial^2 v}{\partial z^2}\right) + \frac{\rho_c}{\rho}\frac{\partial V}{\partial y}, \tag{6}$$

$$u\frac{\partial w}{\partial x} + v\frac{\partial w}{\partial y} + w\frac{\partial w}{\partial z} = -\frac{1}{\rho}\frac{\partial p}{\partial z} + \nu\left(\frac{\partial^2 w}{\partial x^2} + \frac{\partial^2 w}{\partial y^2} + \frac{\partial^2 w}{\partial z^2}\right) + \frac{\rho_c}{\rho}\frac{\partial V}{\partial z}. \tag{7}$$

The last terms on the right-hand side of Navier-Stokes equations (Eqs. (5-7)) are the body forces produced by the electric field. The one-way coupling, which assumes that the electric field can have direct effects on the flow field but not vice versa, has been applied. This assumption, which allows the decoupling of electric field from flow field, has been justified by Huang and Lai [26]. Owing to the symmetry of the problem, only one quarter of the channel was needed for computations. Thus, the corresponding boundary conditions for the flow field are,

On the channel walls,

$x = 0,$	$u = 0,$	$v = 0,$	$w = 0,$	(7a)
$y = 0,$	$u = 0,$	$v = 0,$	$w = 0,$	(7b)

On the symmetric planes,

$x = \frac{D}{2},$	$u = 0,$	$\frac{\partial v}{\partial x} = 0,$	$\frac{\partial w}{\partial x} = 0,$	(7c)
$y = \frac{D}{2},$	$\frac{\partial u}{\partial y} = 0,$	$v = 0,$	$\frac{\partial w}{\partial y} = 0,$	(7d)

At the inlet of the channel,
$$z = 0, \qquad u = u_i, \qquad v = 0, \qquad w = 0, \qquad (7e)$$

At the outlet,
$$z = \frac{H}{D}, \qquad \frac{\partial u}{\partial z} = 0, \qquad \frac{\partial v}{\partial z} = 0, \qquad \frac{\partial w}{\partial z} = 0. \qquad (7f)$$

Computations for the electric field have been performed using an in-house program based on the finite different method. For the electric field calculations, only one quarter of the channel has been used taking advantage of the symmetry of the problem. In addition, it is anticipated that the electric field would not vary significantly further downstream of the bottom grounded plate. As such, a channel length of 40.64 cm (16 in.) has been used in the numerical model to reduce the computational time. A uniform grid of 51 x 51 x 401 has been selected for the present calculations. A numerical algorithm proposed by Yamamoto and Velkoff [3] has been employed for the solution of electric field. In this approach, electric potential and space charge density are determined by iterations with an assumed value of space charge density at the wire tip (ρ_{c0}). The validity of the solution is checked by comparing the predicted total current (Eq. 8) with the measured current at the corresponding voltage in experiment. If the currents do not match, a new value of space charge density at the wire tip is assumed and the calculations are repeated until the calculated total current agrees well with the measured value for that given applied voltage.

$$I_{cal} = 2\int_0^D \int_0^W \rho_c b \left(\frac{\partial V}{\partial x} \right) dydz + 2\int_0^D \int_0^W \rho_c b \left(\frac{\partial V}{\partial y} \right) dxdz, \qquad (8)$$

There are other algorithms for the solution of electric field (e.g., those proposed by McDonald et al. [27] as well as Kalio and Stock [28]), in which the electrical field condition at the wire is estimated by the Peek's semi-empirical formula [29] instead of an assumed value. It should be pointed out that an empirical constant, named the wire condition factor, has been introduced in the formula mentioned above. Since the assignment of this empirical constant is somewhat arbitrary, the approach proposed by Yamamoto and Velkoff [3] is preferred over the later ones [27-28] in this study. However, it has been reported [30-31] that the agreement between the results obtained by these two approaches is very good when the solutions converged.

On the other hand, computations for the flow field have been performed using a commercial code Fluent 6.3.26. After the solution of the electric field converges, electric body forces can be determined and this information is passed on to fluent using its user defined function. A non-uniform grid has been used for the calculations of the flow field. Finer meshes are applied to the region near the wall where the viscous and electric body forces dominate. Relatively coarse meshes are used in the regions far away from the wall and far downstream. A total of 704,000 cells have been used for the computation of flow field. Again, further refinements of the mesh do not appear to produce any significant change in the results, but merely increase the computational time tremendously. All computations have been performed on a 64-bit workstation with 2 GHz CPU and 8 Gb RAM. A typical run takes about seven to ten hours of CPU time for the solution of the electric field. However, the time required to solve for the flow field ranges from three hours to six hours, depending on the applied voltage.

RESULTS AND DISCUSSION

The electric potential distributions inside the test channel are shown in Fig. 4 for an EHD gas pump of Configuration 1 (with a 1.27-cm-wide grounded plate at the top stage) operating at an applied voltage varying from 20 kV to 28 kV at an increment of 2 kV. It is observed that a large potential gradient exists between the wire electrodes and the grounded plate for both top and bottom stages. It also appears that the potential gradient is slightly larger in the top stage than the bottom stage. Below the grounded plate of the bottom stage, the potential does not vary significantly. Hence, it is justified to use a shorter channel length for the electric field calculations. From Fig. 4, one can see that the electrode pins has significantly modified the electric field. This non-uniform electric field is an essential condition for the generation of corona wind.

Space charge density distributions are shown in Fig. 5 for the EHD gas pump with the same configuration operating at the same applied voltages. As observed, space charges are centered at the electrode tips and spread downwards to the grounded plate at both top and bottom stages. Their density reduces significantly when moving away from the tip of emitting electrode. With an increase in the applied voltage, space charges are further confined to a smaller region at the tip. It is interesting to observe that space charges fill up the entire region between the electrode tips and the grounded plate at a lower voltage. However, at an applied voltage of 26 kV and 28 kV, space charges are highly concentrated at the electrode tips, and their density reduces dramatically within a short distance away from the tips.

The distributions of electrica potential and charge density for an EHD gas pump with Configuration 2 (2.54-cm-wide grounded plate at the top stage) and 3 (5.08-cm-wide grounded plate at the top stage) are shown in Figs 6-9. Their characteristics are basically the same as those of Configuration 1. The only difference among them is that their values are smaller when the size of the grounded plate is larger. This is consistent with the V-I curves observed in Fig. 3.

To examine the induced flow produced by the EHD gas pump, the velocity contours are presented in Fig. 10 for the pump of Configuration 1 operating at various applied voltages. As observed, for V_o < 24 kV, the fluid inside the channel is nearly stagnant (notice the extremely small increment in velocity for Fig. 10 (a) and 10 (b)) . Corona wind is not fully in force until the applied voltage increases
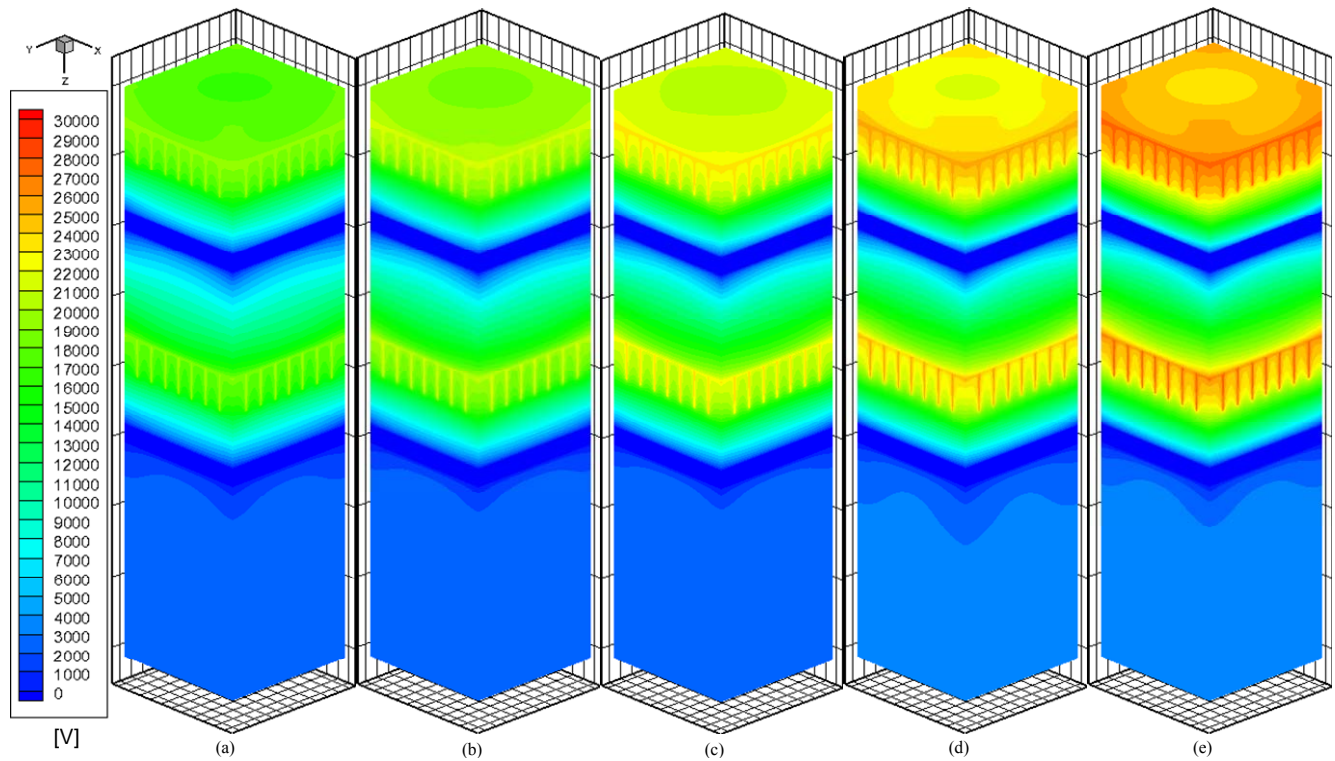
Fig. 4 Distribution of electric potentials in a square channel with a two-stage EHD gas pump operating at various voltages (Configuration 1), (a) $V_o = 20$ kV, (b) $V_o = 22$ kV, (c) $V_o = 24$ kV, (d) $V_o = 26$ kV, (e) $V_o = 28$ kV.
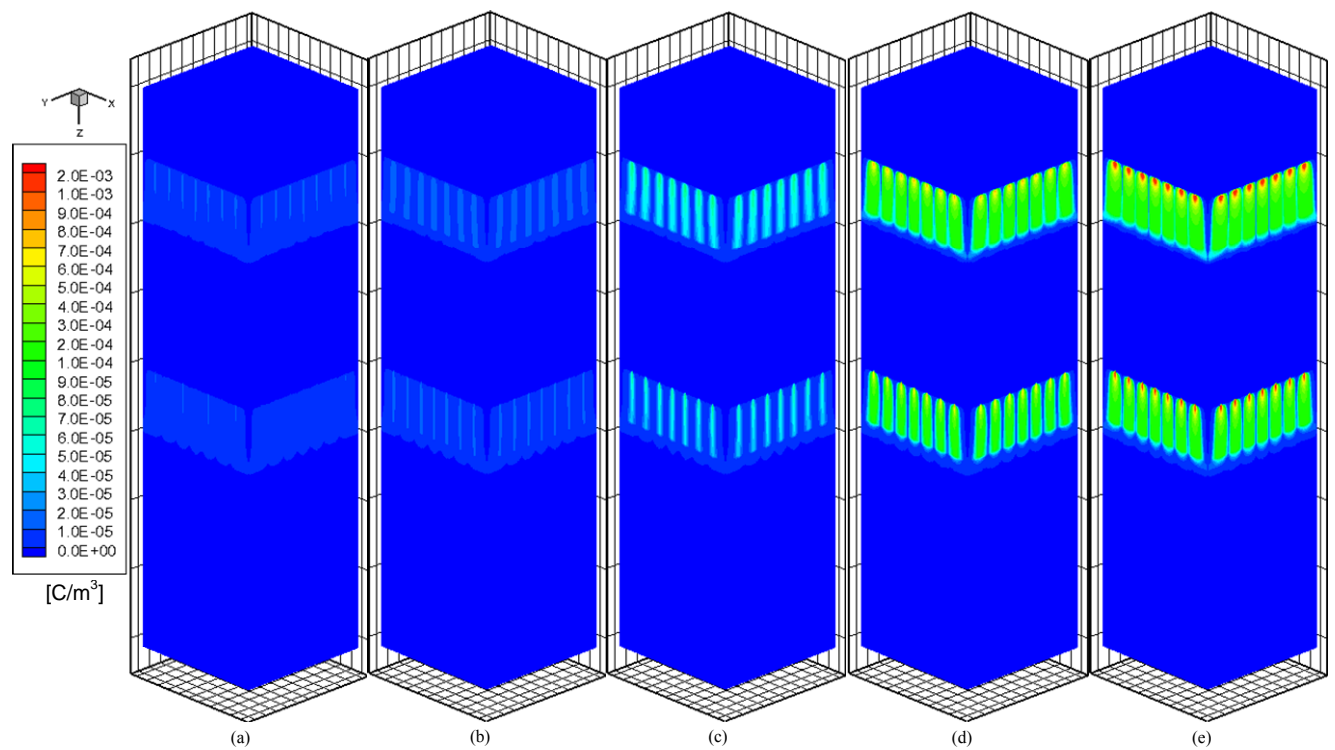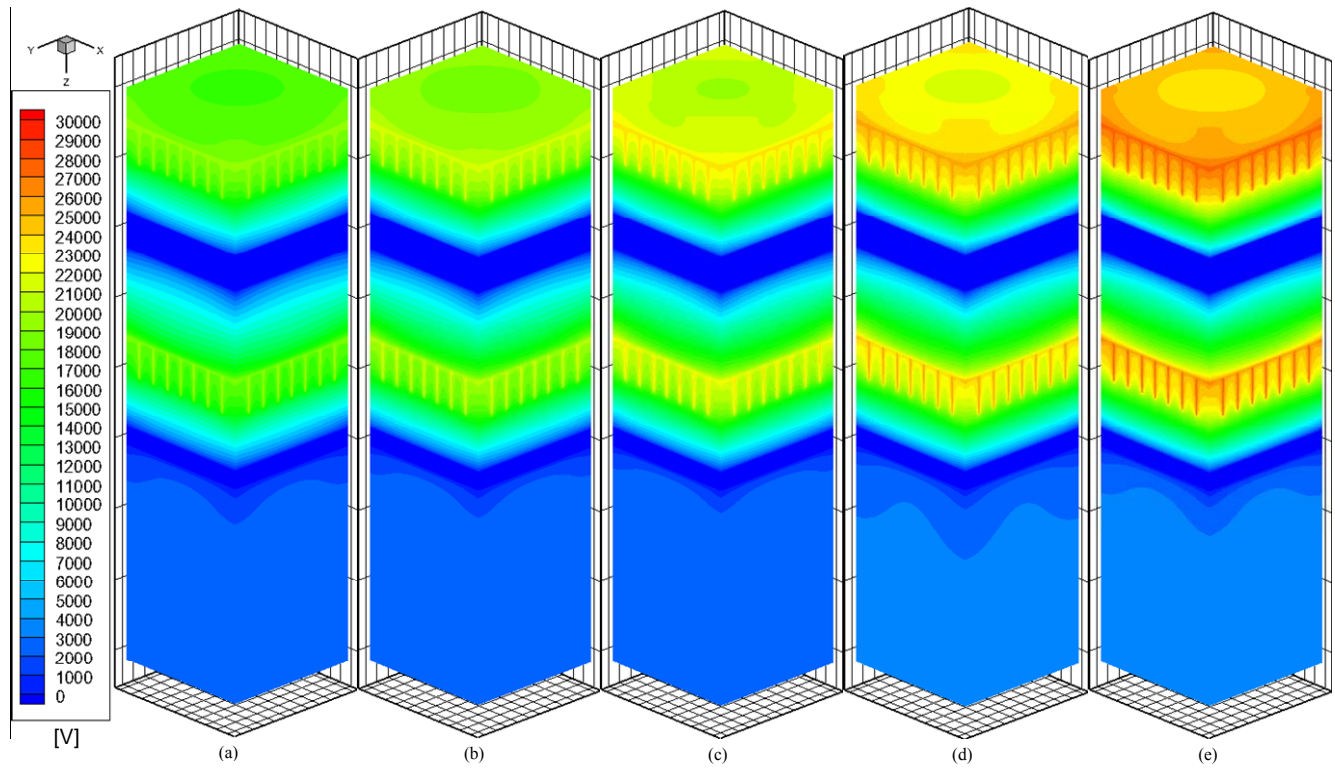

Fig. 5 Distribution of charge density in a square channel with a two-stage EHD gas pump operating at various voltages (Configuration 1), (a) $V_o = 20$ kV, (b) $V_o = 22$ kV, (c) $V_o = 24$ kV, (d) $V_o = 26$ kV, (e) $V_o = 28$ kV.
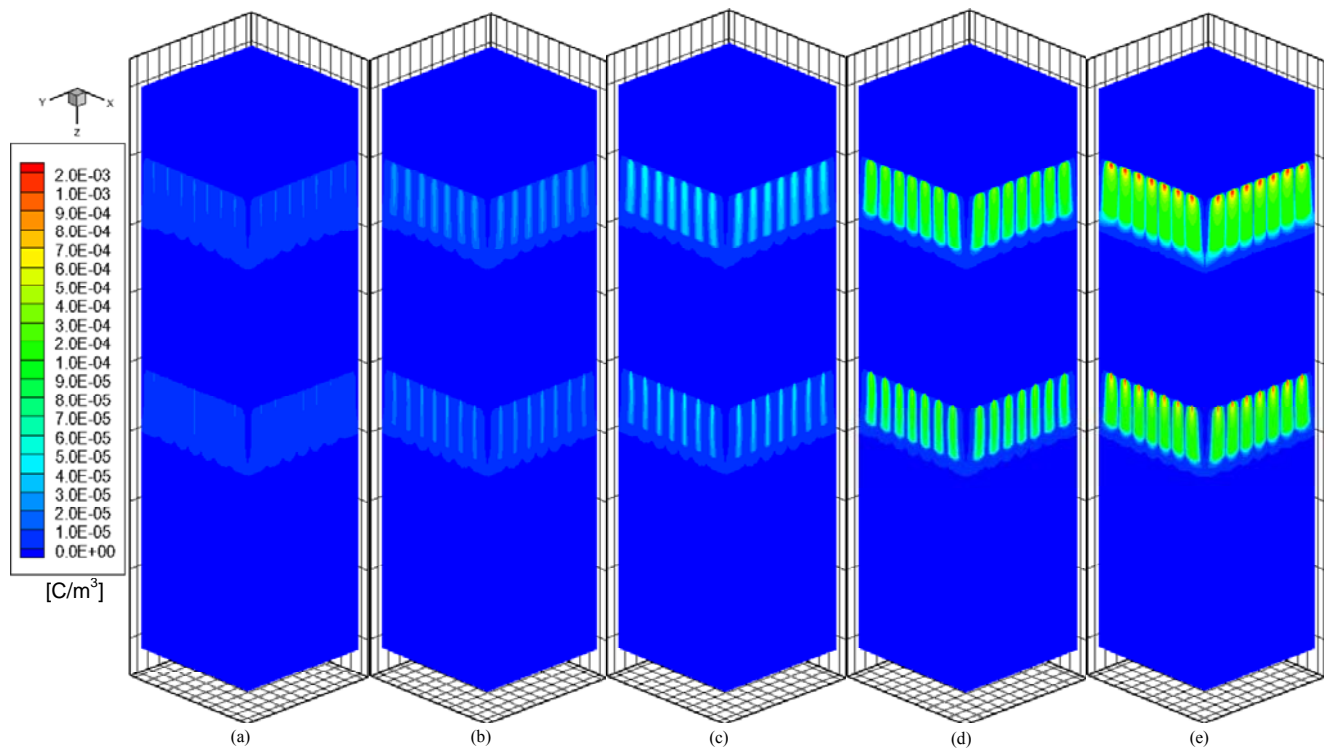
Fig. 6 Distribution of electric potentials in a square channel with a two-stage EHD gas pump operating at various voltages (Configuration 2), (a) $V_o = 20$ kV, (b) $V_o = 22$ kV, (c) $V_o = 24$ kV, (d) $V_o = 26$ kV, (e) $V_o = 28$ kV.

Fig. 7 Distribution of charge density in a square channel with a two-stage EHD gas pump operating at various voltages (Configuration 2), (a) $V_o = 20$ kV, (b) $V_o = 22$ kV, (c) $V_o = 24$ kV, (d) $V_o = 26$ kV, (e) $V_o = 28$ kV.
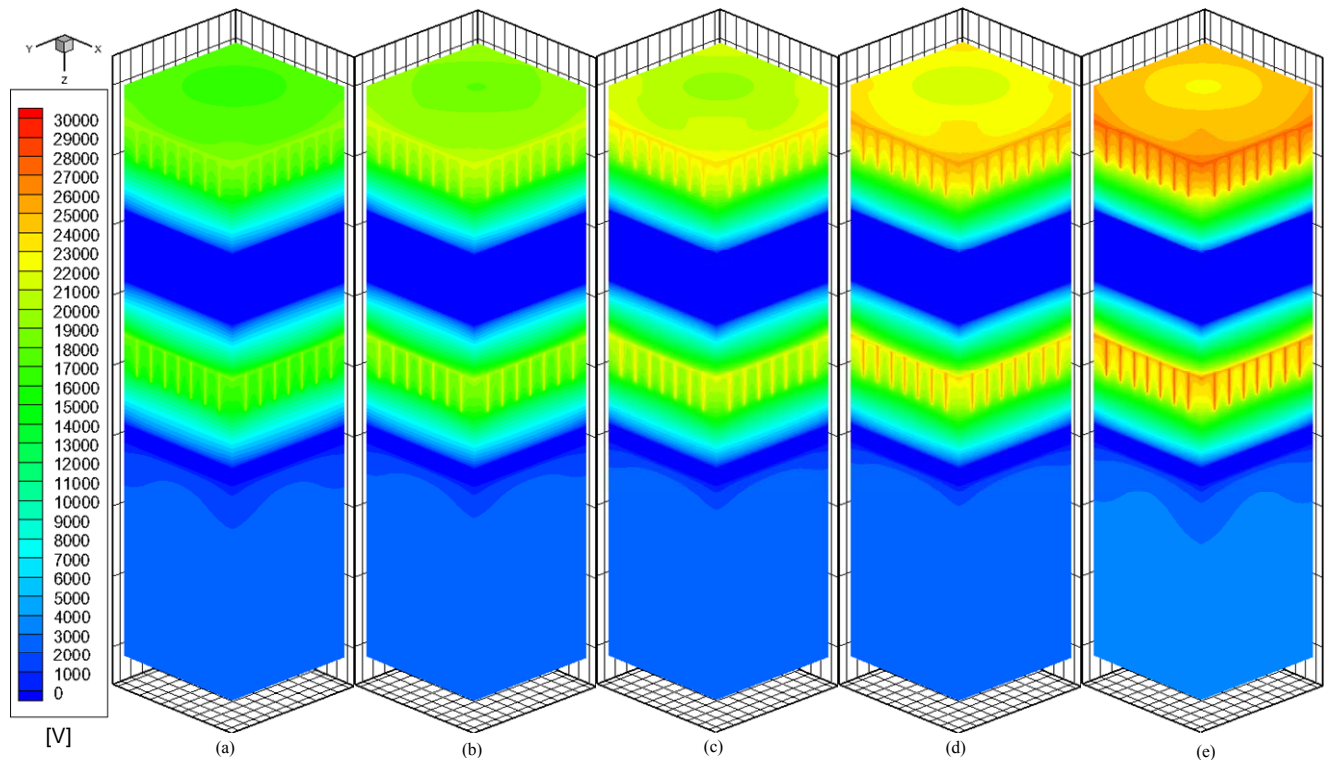
Fig. 8 Distribution of electric potentials in a square channel with a two-stage EHD gas pump operating at various voltages (Configuration 3), (a) V_o = 20 kV, (b) V_o = 22 kV, (c) V_o = 24 kV, (d) V_o = 26 kV, (e) V_o = 28 kV.
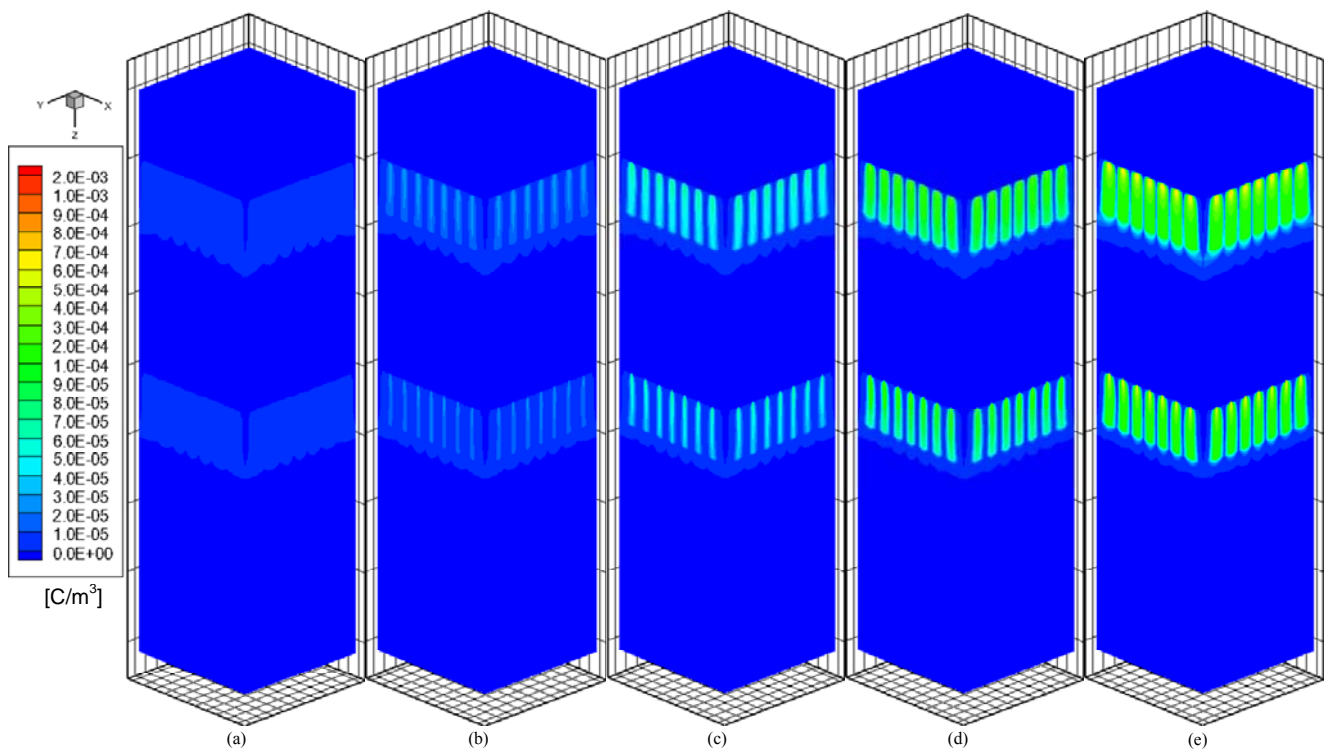

Fig. 9 Distribution of charge density in a square channel with a two-stage EHD gas pump operating at various voltages (Configuration 3), (a) V_o = 20 kV, (b) V_o = 22 kV, (c) V_o = 24 kV, (d) V_o = 26 kV, (e) V_o = 28 kV.

to 24 kV. One clearly sees that corona wind issues from the tip of emitting electrode and it shoots to the center and spread over downstream. Since the emitting electrodes are mounted on the wall, the flow induced by corona wind resembles that of a wall jet. Also observed is that the strength of the corona wind produced from the top stage is stronger than that from the bottom stage. As the applied voltage increases, the corona induced flow continues to develop along the channel wall. From the contour plots shown, the maximum flow velocity appears close to the wall while fluid in the core region of the channel remains nearly stagnant.

The velocity profiles produced by an EHD gas pump with different configurations are shown in Fig. 11 for an applied voltage of 26 kV. As observed, the induced flows all display the same characteristics. They develop along the channel wall leaving the center nearly at rest. One also observes that the induced flow has a slightly higher velocity for EHD gas pump with a smaller size of grounded plate at the top stage (Configuration 1). Again, this is consistent with the V-I characteristics curves (Fig. 3) observed earlier. Since the velocity of corona wind is directly proportional to the corona current it delivers, the EHD gas pump with Configuration 1 has produced the most current, and thus the fastest corona wind.

Figure 12 depicts the velocity profile inside the channel at the cross-section 2.54 cm downstream of the grounded electrode of the bottom stage. In this figure, the x-axis represents the dimensionless channel width so that the locations of $\bar{x} = 0$ and $\bar{x} = 1$ refer to the channel walls. Both experimental measurements and numerical predictions are included in the figure for comparison. While both results do not agree with each other exactly, the trends they showed are consistent.

When the applied voltage is low ($V_o \leq 22$ kV), the velocity profile is fairly uniform across the channel. As the applied voltage increases, the velocity profile looks like an inverted parabola, which is different from that of a fully developed velocity profile for a forced flow inside a channel. This is mainly due to the fact that the emitting electrodes were embedded in the channel wall. The corona wind produced by these electrodes behaves like a wall jet, leading to the maximum air velocity to occur near the wall. This feature is more pronounced when the applied voltage increases beyond 24 kV.

Although one would expect a symmetrical velocity profile, it is observed that the experimental measurement of velocity at $\bar{x} = 0.125$ (x = 1.27 cm or 0.5 in.) is actually
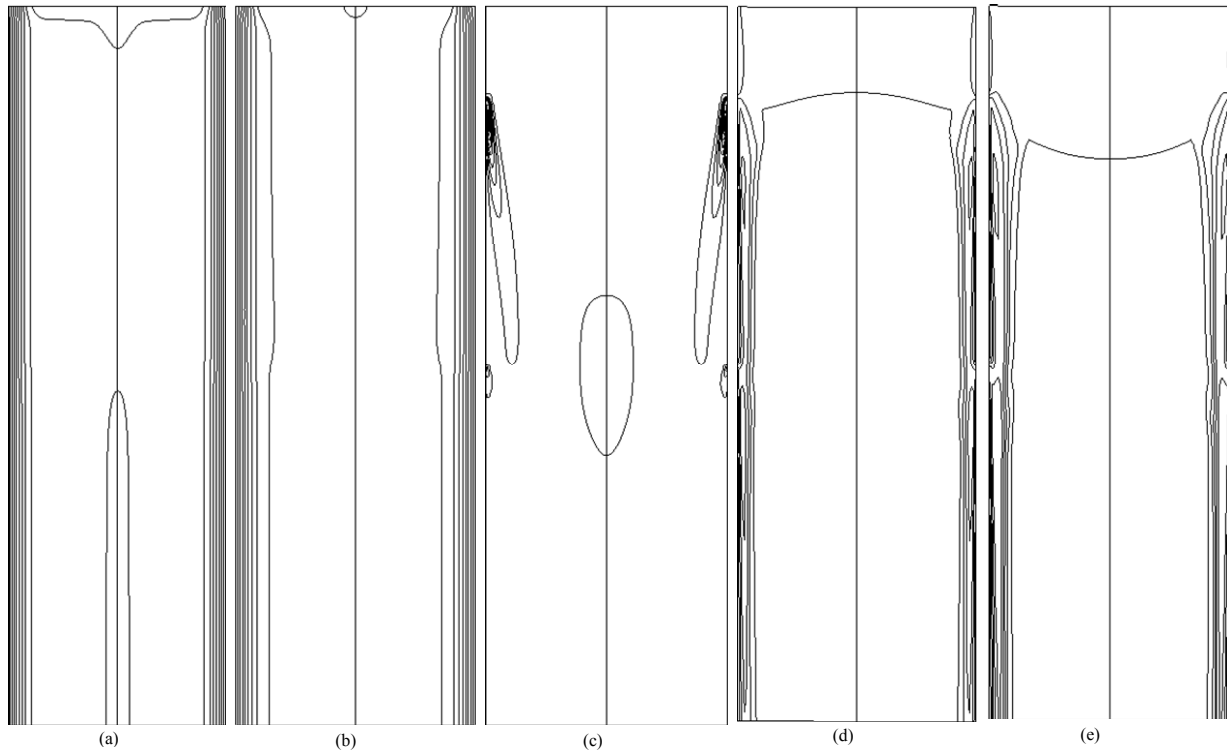

(a)　　　　　(b)　　　　　(c)　　　　　(d)　　　　　(e)

Fig. 10 Velocity contour at the mid-plane of the channel ($\bar{x} = \frac{1}{2}$), Configuration 1, (a) $V_o = 20$ kV ($\Delta u = 0.0001$ ms/), (b) $V_o = 22$ kV ($\Delta u = 0.0001$ ms/), (c) $V_o = 24$ kV ($\Delta u = 0.05$ ms/), (d) $V_o = 26$ kV ($\Delta u = 0.5$ ms/), (e) $V_o = 28$ kV ($\Delta u = 0.5$ ms/).
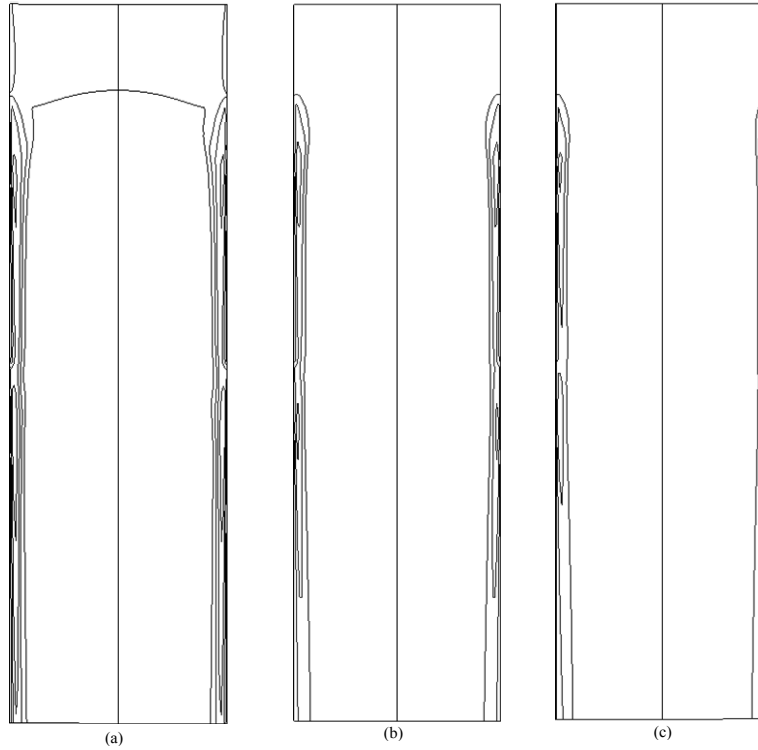
Fig. 11 Velocity contour at the mid-plane of the channel ($\bar{x}$ = ½), V_o = 26 kV (Δu = 0.5 ms/),
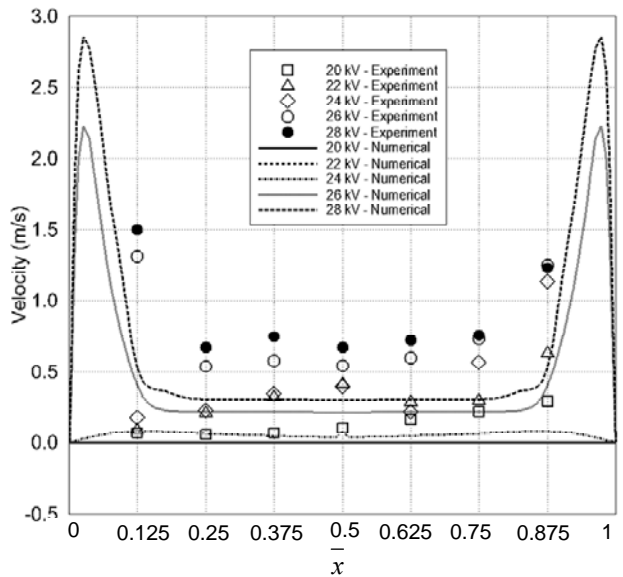(a) Configuration 1, (b) Configuration 2, (c) Configuration 3.

Fig. 12 Velocity profiles at 2.54 cm downstream of the grounded electrode of the bottom stage (Configuration 1).

Fig. 13 Volume flowrate produced by a two-stage EHD gas pump of Configuration 1.

higher than that at $\bar{x}$ = 0.875 (x = 8.89 cm or 3.5 in.). This asymmetric velocity profile is caused by the presence of the velocity measuring probe, which has adversely disturbed the flow. In addition, it is observed that the induced airflow velocity increases with an increase in the applied voltage.
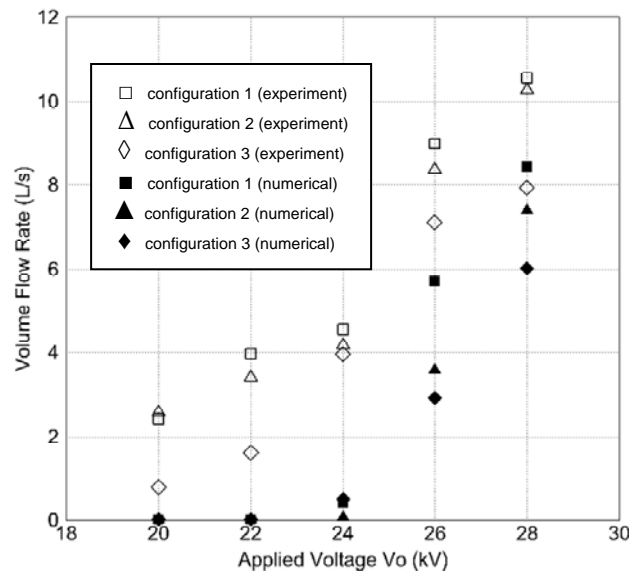
The highest velocity measured in this configuration is as high as 1.5 m/s. The same features hold for velocity profiles at other cross-sections (z = 6.35 cm and z = 10.16 cm) as well as those produced by an EHD gas pump with electrode configurationsof 2 and 3.

It is important to note that the velocity measurements for the present study is quite challenging. Non-intrusive method such as Laser Doppler Velocimetry (LDV), although preferred in most cases, is not ideal for the present study as the seeding particles may be charged by the electric field and affected by Coulomb force. Their velocity and trajectory can thus be compromised. Instead, a hot-wire anemometer was used in the present study with understanding that its intrusion could adversely disturb the flow field, particularly at region close to the wall. In any case, the unique shape of the velocity profile obtained from both results reveals that the corona wind issued from the electrode pins behaves like a wall jet, which can be put to good use in the control of boundary layer development.

The average volume flowrate of air induced by the EHD gas pump is shown in Fig. 13 as a function of applied voltage. Again, both experimental and numerical results are included for comparison. The experimental values are obtained through integrations based on the area-weighted of velocity data. As observed, numerical results always under-predict the volume flowrate. The maximum discrepancy between these two results occurs at a small applied voltage ($V_o < 24$ kV) where numerical simulations essentially predict no flow. Other than this fundamental difference, both results show that the volume flowrate of induced air increases with an increase in the applied voltage. When comparing with the volume flowrate produced by an EHD gas pump with a single stage [25], one finds that the volume flow rate induced by the two-stage EHD gas pump is substantially greater than that of single stage. The maximum volume flow rate observed in this study is 10.5 L/s at an applied voltage of 28 kV.

CONCLUSION

Experimental and numerical studies have been performed for a two-stage electrohydrodynamic (EHD) gas pump operated by positive corona discharge. Since the emitting electrodes are mounted on the inner surface of the channel wall, corona wind issued from these electrodes behaves like a set of wall jets, leading to a higher velocity near the channel walls and resulting in an inverted parabolic velocity profile at the center of the channel. The maximum volume flow rate of air induced by the proposed EHD gas pump can reach as high as 10.5 L/s when operating at a voltage of 28 kV. As far as the performance is concerned, it has been shown that the EHD gas pump proposed is more effective than most conventional fans.

While the present study has only considered an EHD gas pump with two stages of electrodes, the results have clearly shown that its performance is greatly enhanced over that with a single stage. Thus, it confirms that the performance of EHD gas pumps can be further improved with the addition of multi-stage electrodes. Depending on the need of a specific application, an EHD pump can be tailored (in terms of electrode configuration and applied voltage) to achieve the desired outcome.

REFERENCES

[1] Robinson, M., "Movement of air in the electric wind of the corona discharge," *Transactions of the American Institute of Electrical and Electronic Engineers*, vol. 80, pp. 143-150, 1961.

[2] Seyed-Yagoobi, J., "Electrohydrodynamic Pumping of Dielectric Liquids," *Journal of Electrostatics*, vol. 63, pp. 861-869, 2005.

[3] Yamamoto, T., and Velkoff, H. R., "Electrohydro-dynamics in an Electrostatic Precipitator," *Journal of Fluid Mechanics*, vol. 108, pp. 1-18, 1981.

[4] Lai, F. C. and Lai, K. W., "EHD-enhanced Drying with Wire Electrode," *Drying Technology*, vol. 20, pp. 1393-1405, 2002.

[5] Alem-Rajabi, A., and Lai, F. C., "EHD-enhanced Drying of Partially Wetted Glass Beads," *Drying Technology*, vol. 23, pp. 597-609, 2005.

[6] Goodenough, T. I. J., Goodenough, P. W., and Goodenough, S. M., "The Efficiency of Corona Wind Drying and Its Application to the Food Industry," *Journal of Food Engineering*, vol. 80, pp. 1233-1238, 2007.

[7] Léger, L., Moreau, E., Artana, G., and Touchard, G., "Influence of a DC Corona Discharge on the Airflow along an Inclined Flat Plate," *Journal of Electrostatics*, vol. 51, pp. 300-306, 2001.

[8] Vilela Mendes, R., and Dente, J., "Boundary-Layer Control by Electric Fields: A Feasibility Study," *Journal of Fluids Engineering*, vol. 120, pp. 626-629, 1997.

[9] Moreau, E., Artana, G., and Touchard, G., "Surface Corona Discharge along an Insulating Flat Plate in air Applied to Electrohydrodynamically Airflow Control: Electrical Properties," *Electrostatics Conference*, vol. 178, pp. 285-290, 2004.

[10] Moreau, E., Léger, L., and Touchard, G., "Effect of a DC Surface-Corona Discharge on a Flat Plate Boundary Layer for Air Flow Velocity up to 25 m/s," *Journal of Electrostatics*, vol. 64, pp. 215-225, 2006.

[11] Magnier, P., Hong, D., Leroy-Chesneau, A., Pouvesle, J. M., and Hureaua, J., "A DC Corona Discharge on a Flat Plate to Induce Air Movement," *Journal of Electrostatics*, vol. 65, pp. 655-659, 2007.

[12] Ohadi, M. M., Nelson, D. A., and Zia, S., "Heat-transfer enhancement of laminar and turbulent pipe-flow via corona discharge," *International Journal of Heat and Mass Transfer*, vol. 34, pp. 1175-1187, 1991.

[13] Molki, M., Ohadi, M. M., Baumgarten, B., Hasegawa, M., and Yabe, A., "Heat Transfer Enhancement of Airflow in a Channel Using Corona Discharge," *Journal of Enhanced Heat Transfer*, vol. 7, pp. 411-425, 2000.

[14] Molki, M., and Damronglerd, P., 2006, "Electrohydro-dynamic Enhancement of Heat Transfer for Developing Air Flow in Square Ducts," *Heat Transfer Engineering*, vol. 27, pp. 35-45.

[15] Richter, A., Plettner, A., Hofmann, K. A., and Sandmaier, H., "A Micromachined Electrohydrodynamic (EHD) Pump," *Sensors and Actuators a-Physical*, vol. 29, pp. 159-168, 1991.

[16] Tanasomwang, L., and Lai, F. C., "Long-term Ozone Generation from Electrostatic Air Cleaners," *Conference Records of the 1997 IEEE Industry Applications Society 32nd IAS Annual Meeting*, vol. 3, pp. 2037-2044, 1997.

[17] Fouad, L., and Elhazek, S., "Effect of Humidity on Positive Corona Discharge in a 3-electrode System," *Journal of Electrostatics*, vol. 35, pp. 21-30, 1995.

[18] Rickard, M., Dunn-Rankin, D., Weinberg, F., and Carleton, F., "Characterization of Ionic Wind Velocity," *Journal of Electrostatics*, vol. 63, pp. 711-716, 2005.

[19] Tsubone, H., Ueno, J., Komeili, B., Minami, S., Harvel, G. D., Urashima, K., Ching, C. Y., and Chang, J. S., "Flow Characteristics of Wire-non-parallel Plate Electrohydrodynamic Gas Pumps," *Journal of Electrostatics*, vol. 66, pp. 115-121, 2008.

[20] Chang, J. S., Tsubone, H., Chun, Y. N., Berezin, A. A., and Urashima, K., "Mechanism of Electrohydro-dynamically Induced Flow in a Wire-non-parallel Plate Electrode Type Gas Pump," *Journal of Electrostatics*, vol. 67, pp. 335-339, 2009.

[21] Komeili, B., Chang, J. S., Harvel, G. D., Ching, C. Y., and Brocilo, D., "Flow Characteristics of Wire-rod Type Electrohydrodynamic Gas Pump under Negative Corona Operations," *Journal of Electrostatics*, vol. 66, pp. 342-353, 2008.

[22] Moreau, E., and Touchard, G., "Enhancing the Mechanical Efficiency of Electric Wind in Corona Discharges," *Journal of Electrostatics*, vol. 66, pp. 39-44, 2008.

[23] Jewell-Larsen, N. E., Krichtafovitch, I. A., and Mamishev, A. V., "Design and Optimization of Electrostatic Fluid Accelerators," *IEEE Transactions on Dielectrics and Electrical Insulation*, vol. 13, pp. 191-203, 2006.

[24] Laser, D. J., and Santiago, J. G., "A Review of Micropumps," *Journal of Micromechanics and Mircoengineering*, vol. 14, pp. R35-R64, 2004.

[25] Zhang, J., and Lai, F. C., "Effect of Emitting Electrode Number on the Performance of EHD Gas Pump in a Rectangular Channel," *Proceedings of the 2010 Electrostatics Society of America (ESA) Annual Meeting*, 2010.

[26] Huang, M. and Lai, F. C., "Numerical Study of EHD-Enhanced Forced Convection Using Two-Way Coupling," *Journal of Heat Transfer*, vol. 125, pp. 760-764, 2003.

[27] McDonald, J. R., Smith, W. B., Spencer, H. W., and Sparks, L. E., "A Mathematical Model for Calculating Electrical Conditions in Wire-Duct Electrostatic Precipitation Devices," *Journal of Applied Physics*, vol. 48, pp. 2231-2243, 1977.

[28] Kallio, G. A., and Stock, D. E., "Computation of Electrical Conditions Inside Wire-Duct Electrostatic Precipitators Using a Combined Finite-Element, Finite-Difference Technique," *Journal of Applied Physics*, vol. 59, pp. 999-1005, 1985.

[29] Peek, F. W., *Dielectric Phenomenon in High Voltage Engineering*, McGraw-Hill, New York, 1966.

[30] Lai, F. C., Mckinney, P. J., and Davidson, J. H., "Oscillatory Electrohydrodynamic Gas Flows," *Journal of Fluids Engineering*, vol. 117, pp. 491-497, 1995.

[31] Lai, F. C., and Kulkarni, S. S., "Effects of Buoyancy on EHD-Enhanced Forced Convection in a Vertical Channel," *Journal of Thermophysics and Heat Transfer*, vol. 21, pp. 730-735, 2007.